remote sensing

MDPI

Article

Satellite-Observed Hydrothermal Conditions Control the Effects of Soil and Atmospheric Drought on Peak Vegetation Growth on the Tibetan Plateau

Zhengliang Qiu [1,†], Longxiang Tang [1,†], Xiaoyue Wang [2,*], Yunfei Zhang [1], Jianbo Tan [1], Jun Yue [3] and Shaobo Xia [1]

[1] School of Traffic & Transportation Engineering, Changsha University of Science & Technology, Changsha 410114, China; 22101020007@stu.csust.edu.cn (Z.Q.); 22201050157@stu.csust.edu.cn (L.T.); zhang.yunfei@csust.edu.cn (Y.Z.); tanjianbo@csust.edu.cn (J.T.); shaobo.xia@csust.edu.cn (S.X.)
[2] The Key Laboratory of Land Surface Pattern and Simulation, Institute of Geographic Sciences and Natural Resources Research, Chinese Academy of Sciences, Beijing 100101, China
[3] The School of Automation, Central South University, Changsha 410083, China; junyue@csu.edu.cn
* Correspondence: wangxy@igsnrr.ac.cn
† These authors contributed equally to this work.

Abstract: Recent research has demonstrated that global warming significantly enhances peak vegetation growth on the Tibetan Plateau (TP), underscoring the influence of climatic factors on vegetation dynamics. Nevertheless, the effects of different drought types on peak vegetation growth remain underexplored. This study utilized satellite-derived gross primary productivity (GPP) and the normalized difference vegetation index (NDVI) to assess the impacts of soil moisture (SM) and vapor pressure deficit (VPD) on peak vegetation growth (GPP_{max} and $NDVI_{max}$) across the TP from 2001 to 2022. Our findings indicate that $NDVI_{max}$ and GPP_{max} exhibited increasing trends in most regions, displaying similar spatial patterns, with 65.28% of pixels showing an increase in $NDVI_{max}$ and 72.98% in GPP_{max}. In contrast, the trend for SM primarily showed a decrease (80.86%), while VPD showed an increasing trend (74.75%). Through partial correlation analysis and ridge regression, we found that peak vegetation growth was significantly affected by SM or VPD in nearly 20% of the study areas, although the magnitude of these effects varied considerably. Furthermore, we revealed that hydrothermal conditions modulated the responses of peak vegetation growth to SM and VPD. In regions with annual precipitation less than 650 mm and an annual mean temperature below 10 °C, decreased SM and increased VPD generally inhibited peak vegetation growth. Conversely, in warm and humid areas, lower SM and higher VPD promoted peak vegetation growth. These findings are crucial for deepening our understanding of vegetation phenology and its future responses to climate change.

Keywords: peak vegetation growth; drought; soil moisture; vapor pressure deficit; Tibetan Plateau

Citation: Qiu, Z.; Tang, L.; Wang, X.; Zhang, Y.; Tan, J.; Yue, J.; Xia, S. Satellite-Observed Hydrothermal Conditions Control the Effects of Soil and Atmospheric Drought on Peak Vegetation Growth on the Tibetan Plateau. *Remote Sens.* **2024**, *16*, 4163. https://doi.org/10.3390/rs16224163

Academic Editors: Junhu Dai and Chung-Te Chang

Received: 9 October 2024
Revised: 2 November 2024
Accepted: 6 November 2024
Published: 8 November 2024

1. Introduction

The Tibetan Plateau (TP), often referred to as the "third pole" of the world, has typical alpine ecosystems that are particularly prone to the repercussions of climate change [1]. During recent decades, the plateau has witnessed a temperature increase at a rate double that of the global average, severely impacting the timing and vigor of vegetation growth [2]. Such changes are critical because alpine vegetation is integral to the carbon and water cycles, influencing the overall climate dynamics [3,4]. Moreover, shifts in vegetation growth can feed back into broader climatic patterns, making it essential to monitor and understand these dynamics for future climate modeling [5–8].

Peak vegetation growth is a main indicator reflecting the carbon absorption capacity of terrestrial ecosystems and regulating the seasonal variation in atmospheric CO_2 concentrations [9–13]. Numerous satellite observations suggest that the Earth's land has been experiencing increased vegetation coverage since the early 1980s [14,15], with an increase in

peak vegetation growth also being perceived globally [12], which has significantly changed the carbon–water cycles within terrestrial ecosystems [16,17]. Research has demonstrated that climatic factors such as precipitation, temperature, and radiation dominate peak vegetation growth [18–22]. Furthermore, CO_2 and nitrogen deposition are crucial in controlling peak vegetation growth [12]. Ongoing global warming is leading to increasingly frequent and prolonged drought events, placing significant stress on ecosystems and potentially resulting in severe ecological imbalances, which profoundly affect vegetation growth [23–28]. Existing research has shown that the sensitivity of phenology to drought has significantly increased in recent decades. Under future climate change scenarios, drought is expected to become more severe and frequent, exacerbating its impact on vegetation [29,30].

Insufficient soil moisture (SM) and elevated atmospheric water requirements, characterized by vapor pressure deficit (VPD), are recognized as the two major factors contributing to drought stress in plants [31]. Soil drought can occur when soil moisture (SM) is insufficient. SM typically refers to the soil humidity or soil water content, which is one of the key factors determining plant growth and hydrological processes. Vapor pressure deficit (VPD) describes the difference between the moisture content in the air and the potential evaporation, characterizing the degree of air dryness, which is crucial for plant transpiration and water exchange. The effects of moisture stress may be exacerbated in the context of ongoing climate warming, complicating our understanding of how the coupling of SM and VPD influences vegetation [32]. Several studies have demonstrated the importance of SM in mediating the exchange of water, energy, and carbon between soil and vegetation, thus influencing the growth conditions of plants [31,33]. However, other research has indicated that VPD, instead of SM, dominates the efficiency of the ecosystem production at more flux sites and on a greater scale globally [34]. For example, Zhong et al. [35] revealed the important role of VPD in terrestrial ecosystems and indicated that increasing VPD would threaten high-latitude ecosystems in the context of continuing global warming. The relative roles of SM and VPD in influencing ecosystem productivity remain highly controversial. Recent studies have indicated that SM is the primary moisture constraint on the productivity of terrestrial vegetation ecosystems in most regions of China, with the rate of increase in SM's impact on vegetation productivity outpacing that of VPD [36]. Conversely, other researchers have found that VPD exerts a greater influence on the productivity of terrestrial ecosystems in China than SM, suggesting that VPD has a stronger and more widespread effect on the trends and variability in ecosystem productivity in the region [37]. Therefore, there is still a lack of consensus regarding the specific impacts of VPD and SM on vegetation productivity at the ecosystem scale, highlighting the need for further investigation into how soil and atmospheric drought affect vegetation growth peaks.

To address this issue, we first derived the maximum values of gross primary productivity (GPP_{max}) and the normalized difference vegetation index ($NDVI_{max}$) as proxies of peak vegetation growth based on remote sensing data from 2001 to 2022 over the TP. Then, we examined the responses of GPP_{max} and $NDVI_{max}$ to SM and VPD. We aimed to answer several questions in our study: (1) What are the relationships between peak vegetation growth and soil and atmospheric drought? (2) What are the spatiotemporal patterns of these relationships? (3) How do such relationships vary among vegetation types and hydrothermal conditions?

2. Data and Methods

2.1. Study Area

The Tibetan Plateau, situated in Central Asia, holds the distinction of being the largest and highest plateau globally, covering much of southwestern China and most of the Tibet Autonomous Region. Its geographic coordinates range from 25°N to 40°N in latitude and 70°E to 105°E in longitude. Boasting an average elevation exceeding 4000 m, the TP surpasses many regions, leading to unique climatic and ecological characteristics. Because of its low latitude, high elevation, and intricate topography, the TP is characterized by its cold temperatures and scant precipitation. From 2001 to 2022, the mean annual temperature varied from −14 °C in the northern part to 24 °C in the southern part (Figure 1b). The

majority of the area is subject to arid or semi-arid climates, with the total annual precipitation typically falling below 1000 mm in most regions (Figure 1c). The vegetation types and distributions in the TP are diverse, enriched and complicated by the variations in geographical conditions and altitudes. Alpine steppe and alpine meadows represent the predominant vegetation types, constituting 27.94% and 25.57% of the region, respectively. They are mainly distributed across the western, midland, and eastern regions of the TP. The vegetation primarily consists of shrubs in the eastern and southern regions, while alpine sparse vegetation is scattered throughout the entire area.

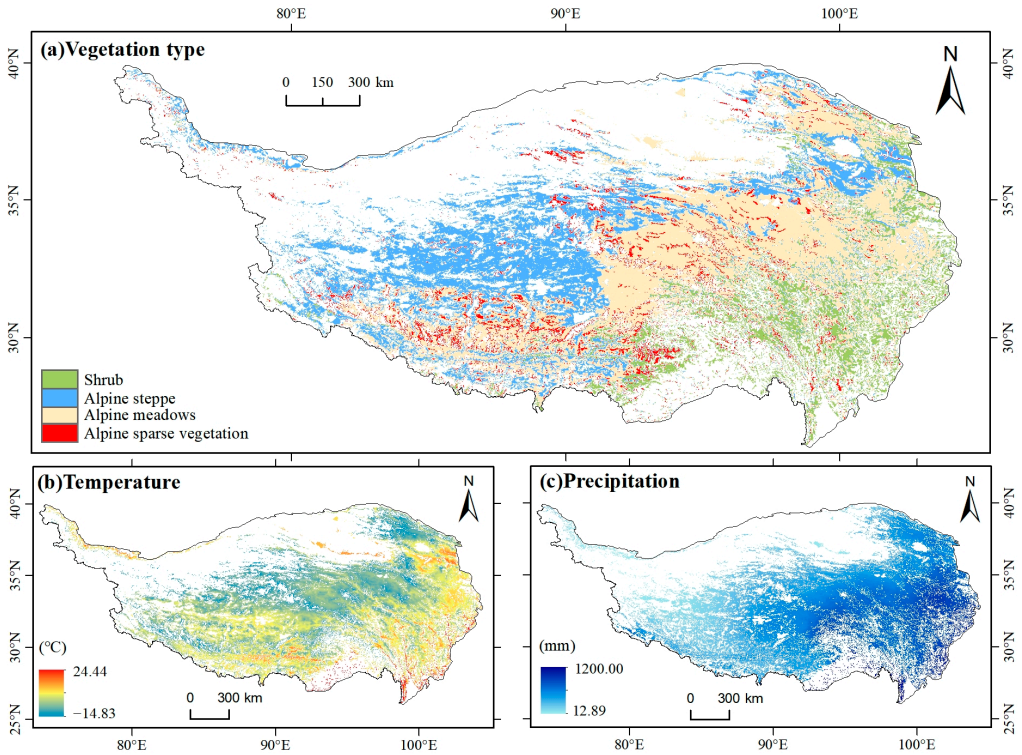

Figure 1. Major features of TP: (**a**) representative vegetation cover types; (**b**) total average temperature from 2001 to 2022; and (**c**) average precipitation from 2001 to 2022.

2.2. Data

2.2.1. NDVI Data

The NDVI, also known as the normalized difference vegetation index, can differentiate vegetation from water and soil, providing an objective reflection of changes in vegetation coverage. It is the optimal indicator of vegetation growth status and coverage. In this study, 500 m spatial resolution MODIS data, MOD13A1 (v061), with a temporal resolution of 16 days and a time span of 22 years (2001–2022), were acquired from the NASA Earthdata Cloud (https://appeears.earthdatacloud.nasa.gov/, accessed on 12 December 2023) website. This dataset comprised two major vegetation layers, the NDVI and EVI, and the NDVI layer was chosen for download. The dataset offered temporal continuity and extensive coverage, making it highly suitable for this research. Then, by setting the NDVI annual average threshold to 0.1, the pixels with an NDVI annual average below 0.1 were excluded. This approach effectively removes areas of low or sparse vegetation, bare soil, and water bodies, thus ensuring the accuracy of the results [38–40]. This threshold was selected to enhance the reliability of the analysis by ensuring that only the areas with healthy vegetation cover were considered in order to obtain more accurate research outcomes.

2.2.2. GPP Data

Gross primary productivity (GPP) is a crucial ecological indicator used to measure the extent to which plants fix solar energy in an ecosystem. It represents the overall productivity and

energy conversion efficiency of an ecosystem and is vital in its energy flow and material cycling. For this research, 500 m spatial resolution MODIS data, MOD17A2H (v061), with a temporal resolution of 8 days and a time span of 22 years (2001–2022), were acquired from the NASA Earthdata Cloud (https://appeears.earthdatacloud.nasa.gov/, accessed on 12 December 2023). The dataset consisted of three major layers: gross primary productivity, net photosynthesis, and quality control indicators. For this study, the gross primary productivity layer was selected for download. To facilitate this research, regions with a multiyear average normalized difference vegetation index (NDVI) below 0.1 were also excluded from the GPP data.

2.2.3. Climate Data

Climate data including SM, VPD, precipitation, temperature, and radiation were obtained from the TerraClimate dataset (https://www.climatologylab.org/terraclimate.html, accessed on 12 December 2023). The spatial resolution was 1/24°. The dataset was developed by the University of California, Merced [41]. To ensure consistency in spatial resolution with the NDVI and GPP data, the meteorological data underwent resampling using the bilinear interpolation method. Similarly, the climate data also eliminated regions with multiple-year mean NDVI values under 0.1. Since the available temperature data only included the maximum and minimum temperature, we took the average of these two variables as the temperature variable for analysis.

2.3. $NDVI_{max}$ and GPP_{max} Extraction Methods

For the NDVI and GPP data, taking the NDVI as an example, we extracted the maximum value for each pixel from all NDVI data over the course of a year, which is designated as $NDVI_{max}$. In this way, each pixel value in the composite image represents the maximum NDVI value for that location across all images throughout the year.

2.4. Statistical Analysis Strategy

First, we conducted a statistical analysis using Theil–Sen median trend analysis [42] (Equation (1)) to examine the trends in $NDVI_{max}$, GPP_{max}, SM, and VPD in the TP district from 2001 to 2022. Next, we assessed the significance ($p < 0.05$) of the trends using the Mann–Kendall test (Equations (2)–(5)). In the following, the formulas and principles are explained, taking $NDVI_{max}$ as an example.

$$\beta = Median\left(\frac{x_j - x_i}{j - i}\right) \qquad \forall j > i \tag{1}$$

$$Z = \begin{cases} \frac{S}{\sqrt{Var(S)}} & (S > 0) \\ 0 & (S = 0) \\ \frac{S+1}{\sqrt{Var(S)}} & (S < 0) \end{cases} \tag{2}$$

$$S = \sum_{i=1}^{n-1} \sum_{j=i+1}^{n} sgn(x_j - x_i) \tag{3}$$

$$sgn(x_j - x_i) = \begin{cases} 1 & if(x_j - x_i) > 0 \\ 0 & if(x_j - x_i) = 0 \\ -1 & if(x_j - x_i) < 0 \end{cases} \tag{4}$$

$$Var(S) = \frac{n(n-1)(2n+5)}{18} \tag{5}$$

where x_i and x_j represent the values of $NDVI_{max}$ for the i-th and j-th years, respectively. A value exceeding 0 denotes a tendency toward increase, whereas a value below 0 signifies a tendency toward decrease. The parameter n represents the length of the time series data, while the function *sgn* corresponds to the sign function. In this research, we evaluated the significance of the tendency changes at a confidence level of $\alpha = 0.05$. A trend was considered

significant when $Z > 1.96$, indicating that the data trend change was statistically significant. Conversely, when $Z < 1.96$, the data trend change was not statistically significant.

Subsequently, this study employed partial correlation analysis to assess the separate impacts of SM and VPD on $NDVI_{max}$. When multiple influencing factors were present, the partial correlation analysis enabled us to isolate the impacts of specific factors by controlling the impacts of the additional variables. To calculate the partial correlation coefficient (Equation (7)), we first needed to compute the simple correlation coefficient (Equation (6)). Using the obtained simple correlation coefficients, we calculated the first-order partial correlation coefficients, as shown below:

$$R_{xy} = \frac{\sum_{i=1}^{n}[(x_i - \overline{x}) \times (y_i - \overline{y})]}{\sqrt{\sum_{i=1}^{n}(x_i - \overline{x})^2}\sqrt{\sum_{i=1}^{n}(y_i - \overline{y})^2}} \quad (6)$$

$$R_{xy,z} = \frac{R_{xy} - R_{xz}R_{yz}}{\sqrt{(1 - R_{xz}^2)}\sqrt{\left(1 - R_{yz}^2\right)}} \quad (7)$$

where $\overline{x}$ and $\overline{y}$ represent the multiyear average of data x and data y, R_{xy} represents the simple correlation coefficient between data x and data y, and $R_{xy,z}$ represents the partial correlation coefficient between data x and data y after excluding the influence of data z. $R_{xy,z} > 0$ and $R_{xy,z} < 0$, respectively, indicate a positive and negative correlation between data x and data y.

The partial correlation analysis conducted in this research comprised four main scenarios: (a) assessing the partial correlation between $NDVI_{max}$ and SM while excluding the impacts of VPD, precipitation, temperature, and radiation; (b) investigating the partial correlation between $NDVI_{max}$ and VPD while excluding the impacts of SM, precipitation, temperature, and radiation; and (c) this article also calculated the partial correlations between $NDVI_{max}$ and other factors. In order to comprehend the mechanisms underlying the impact of SM and VPD on $NDVI_{max}$, we initially examined the response of $NDVI_{max}$ to variations in SM. Subsequently, we compared the response of $NDVI_{max}$ to changes in VPD to determine the primary factor influencing $NDVI_{max}$. Similar analyses were conducted for GPP_{max}.

Furthermore, to maximize the correlation, we performed the following process [42–44] when obtaining the partial correlation coefficient between $NDVI_{max}$ and a factor: First, we obtained the maximum value of the NDVI for every year; then, we determined the month in which the NDVI reached its maximum value; and finally, we obtained the median as the final result month for this cell. If $NDVI_{max}$ occurred in June, we calculated the partial correlation coefficients between $NDVI_{max}$ and SM in June and the average SM in June–May, June–April, June–March, June–February, and June–January. The control variable in the partial correlation was the average VPD of the same period. If the absolute value of the partial correlation coefficient between $NDVI_{max}$ and the average SM for April to June was the highest, then the preseason length of the pixel SM was 2 months (zero in the current month); this represented the ultimate partial correlation coefficient between $NDVI_{max}$ and SM for the pixel.

In addition to calculating the partial correlation coefficients of $NDVI_{max}$ with SM and VPD, we also calculated the partial correlation coefficients of $NDVI_{max}$ with three other meteorological factors. To better elucidate the impact of each meteorological factor on peak vegetation growth, we determined the strongest correlated meteorological factor for each pixel location using the maximum absolute value of the partial correlation coefficients.

In addition, this study also employed ridge regression analysis due to the collinearity issues among the climate factors [45–47]. This is a biased estimation regression method specifically designed for analyzing collinear data. We first normalized the data and input them into the ridge regression model. Then, we used generalized cross-validation to select the optimal parameters for the ridge regression model [45,48]. The explanatory variables in this study are the climate factors on an annual scale, including SM, VPD, temperature, precipitation, and radiation, while the dependent variable is $NDVI_{max}$. The coefficient of the ridge regression is used as the intensity of the sensitivity [40,49]. By identifying the

results with the largest absolute values of the ridge regression coefficients, we obtained the climate factor with the greatest sensitivity to $NDVI_{max}$ for each pixel location.

$$\theta(\alpha) = \left(X^T X + \alpha I\right)^{-1} X^T y \tag{8}$$

$$X_{norm} = \frac{x - min(x)}{max(x) - min(x)} \tag{9}$$

$$Y_{norm} = \sum_{i=1}^{n} a_i x_{inorm} + b \tag{10}$$

where $\theta(\alpha)$ represents the analytical solution for the ridge regression coefficients, allowing for the direct calculation of the regression coefficients. α_i is a regularization term. Typically, the appropriate α value is selected through generalized cross-validation to find the best model performance. X_{norm} represents the standardization of the data, including vegetation peak, $NDVI_{max}$, and meteorological factors such as SM, VPD, temperature, precipitation, and radiation. Y_{norm} represents the standardized $NDVI_{max}$, x_{inorm} represents the standardized climate factors, and a_i represents the ridge regression coefficients.

3. Results

3.1. Spatial and Temporal Patterns of $NDVI_{max}$ and GPP_{max}

The spatial patterns and trends of $NDVI_{max}$ from 2001 to 2022 are shown in Figure 2. Spatially, the high $NDVI_{max}$ values were dispersed in the southeastern region, while the low values were dispersed in the northwestern region. The areas with $NDVI_{max}$ values ranging from 0.1 to 0.4 comprised 43.08% of the total area (Figure 2a). In the results of the $NDVI_{max}$ standard deviation calculation, the vast majority of the area (88.63%) comprised values ranging from 0 to 0.06, while only a few regions exhibited high values, which were mostly in the northeastern and southern areas (Figure 2b). Based on the Theil–Sen slope estimation and the Mann–Kendall trend test, $NDVI_{max}$ demonstrated an increasing trend from 2001 to 2022 (Figure 2c). Approximately 16.35% of the pixel area showed a significant upward trend. The area with a significant increase in pixels was more than five times greater than the area with a significant decrease (Figure 2c).

GPP_{max} displayed a spatial pattern similar to $NDVI_{max}$, with the high GPP_{max} values primarily scattered across the eastern TP. Conversely, the GPP_{max} values exhibited in the western regions were generally low: the overall average was 0.52 g C/m^2 (Figure 2d). The spatial distribution of the GPP_{max} standard deviation mirrored that of the mean, with the elevated values observed in the eastern regions and the lower values in the western areas. The regions with values ranging from 0 to 0.1 g C/m^2 covered 83.60% of the area (Figure 2e). From 2001 to 2022, GPP_{max} showed an increasing trend (Figure 2f). Roughly 16.68% of the pixels demonstrated a notable upward trend, while 0.86% showed a significant downward trend (Figure 2f).

3.2. Spatial and Temporal Patterns of SM and VPD

SM and VPD exhibited distinct spatial patterns over the multiyear average (Figure 2g,j). From 2001 to 2022, the spatial distribution of SM was analogous to that of $NDVI_{max}$ and GPP_{max}. The SM values were elevated in the eastern and southern areas of the TP, whereas they were lower in the western and northern regions, with the areas ranging from 0 to 60 m^3/m^3 accounting for 75.45% of the total area (Figure 2g). The standard deviation of SM was generally low, with only some values exceeding 28 mm in the eastern, southern, and western-central areas, and the proportion with 0–28 mm was 98.49% (Figure 2h). A declining tendency in SM was noticed during the period from 2001 to 2022, with an average rate of −0.19 mm/year (Figure 2i). Notably, approximately 25.82% of the pixel zone exhibited a noticeable decreasing tendency, which was 10 times greater than the region displaying a prominent increasing tendency (Figure 2i).

The spatial patterns and tendencies of VPD from 2001 to 2022 are depicted in Figure 2j–l. The results indicated an overall low VPD with only some regions in the northeastern area of the TP showing slightly higher VPD values, with an average of 0.53 kPa (Figure 2j). The spatial distribution of the standard deviation of VPD was similar to its mean value. Except for the northeastern region, which was slightly higher, the remaining regions were generally lower, and the regions with a value between 0 and 36 kPa accounted for 95.67% of the area (Figure 2k). Approximately 74.75% of the pixel regions exhibited an increasing tendency in VPD during the period from 2001 to 2022 (significant at 31.86%), which were mainly concentrated in the central, western, and northeastern regions of the TP. Conversely, the eastern and northern areas showed a decreasing trend, with the significant trends accounting for 2% of the pixel regions (Figure 2l).

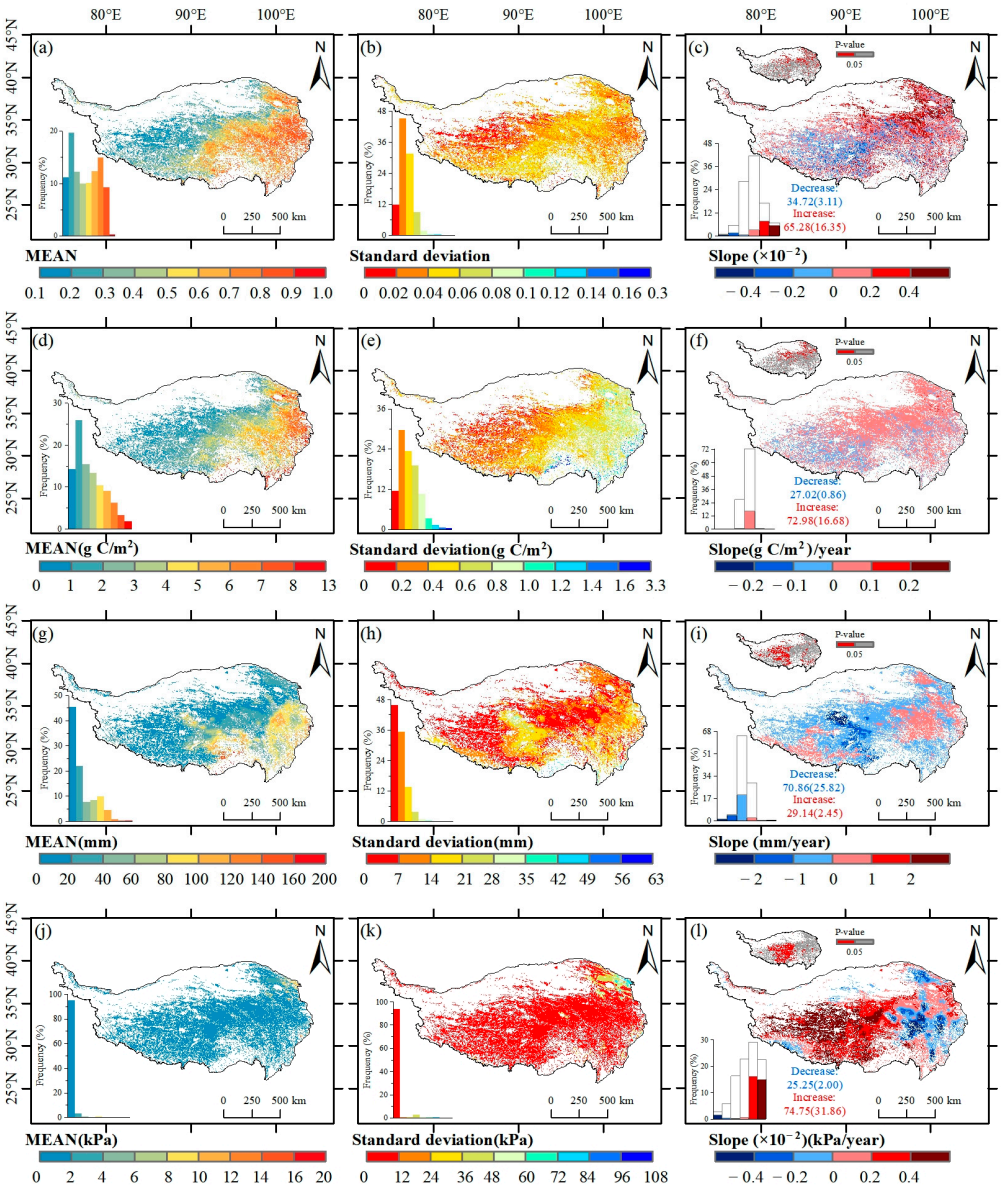

Figure 2. The spatial distributions of the multiyear averages (**a**,**d**,**g**,**j**), standard deviations (**b**,**e**,**h**,**k**), and temporal trends and significance levels (**c**,**f**,**i**,**l**) of the normalized vegetation index ($NDVI_{max}$), gross primary productivity (GPP_{max}), soil moisture (SM), and vapor pressure deficit (VPD) on the TP. The subplots (**a**,**b**,**d**,**e**,**g**,**h**,**j**,**k**) include their respective frequency distributions. The small insets at the top of (**c**,**f**,**i**,**l**) show the areas with significant trends ($p < 0.05$), where the bar charts represent the frequency distribution of the trends, the colored bars indicate the significant trends, and the white bars indicate the nonsignificant trends.

3.3. Response of $NDVI_{max}$ and GPP_{max} to Climate Data

After controlling for the effects of SM, temperature, precipitation, and radiation, a negative correlation between $NDVI_{max}$ and VPD was noted in the TP. Notably, approximately 11.51% of the significant negative correlations were mostly in the northeast and southwest areas, while a significant positive correlation of 8.38% was observed (Figure 3a). This suggested an overall detrimental effect of higher VPD on $NDVI_{max}$. Conversely, upon eliminating the impacts of VPD, temperature, precipitation, and radiation, roughly 57.46% of the pixels exhibited a positive relationship with SM, with 12.61% indicating a significant positive correlation ($p < 0.05$, Figure 3b). These regions were primarily scattered across the eastern, central, and southwestern areas of the TP. Instances of significant negative correlations were less prevalent (6.59%) and were mostly observed in some central and western regions. This implied that higher SM was conducive to vegetation growth in the central TP.

Compared with $NDVI_{max}$, GPP_{max} displayed similar responses to VPD and SM. After the influence of SM, temperature, precipitation, and radiation was mitigated, GPP_{max} exhibited a negative correlation with VPD. Among the significant correlations (18.29%), negative associations accounted for 61.55% (Figure 3c). These notable negative correlations were mainly observed in the central and northeastern portions of the TP, indicating an overall adverse effect of higher VPD on GPP_{max}. Conversely, after the effects of VPD, temperature, precipitation, and radiation were eliminated, GPP_{max} exhibited a positive correlation with SM. Approximately 19.21% of the pixels within the research region demonstrated a significantly biased correlation (Figure 3d), among which 12.65% displayed a notable positive correlation, and were mostly in the central and eastern regions. The remaining pixels exhibited a notable negative correlation (6.57%). This finding underscores the favorable impact of elevated SM on GPP_{max}.

As can be seen from Figure 3, temperature, precipitation, and radiation played important roles in both $NDVI_{max}$ and GPP_{max}, which is consistent with other research results. Furthermore, from the distributions in the figures and the bar charts, it is evident that among the meteorological factors most strongly correlated with $NDVI_{max}$, SM accounted for 16.83% and VPD accounted for 16.85% (Figure 3e). For the meteorological factors most strongly correlated with GPP_{max}, SM accounted for 12.38% and VPD accounted for 13.49% (Figure 3f). It can be seen that the correlation between SM and VPD on peak vegetation growth was as important as precipitation and radiation.

Figure 4 shows the ridge regression coefficients for the regions with significant partial correlation coefficients, which represent the intensity of the sensitivity. It can be seen that the spatial distribution of the sensitivities of SM and VPD to $NDVI_{max}$ was similar to the spatial distribution of the partial correlation, and the distribution of GPP_{max} also showed a similar trend (Figure 4a–d). Furthermore, when comparing the sensitivities of the various meteorological factors to vegetation growth peaks, SM accounted for 15.76% of the most sensitive factors for $NDVI_{max}$, while precipitation accounted for 17.55% (see Figure 4e). For GPP_{max}, SM represented 15.55%, and precipitation accounted for 11.12% (see Figure 4f). This indicates that the sensitivities of SM and precipitation to vegetation growth peaks are consistent, further supporting the results of the strongest correlation.

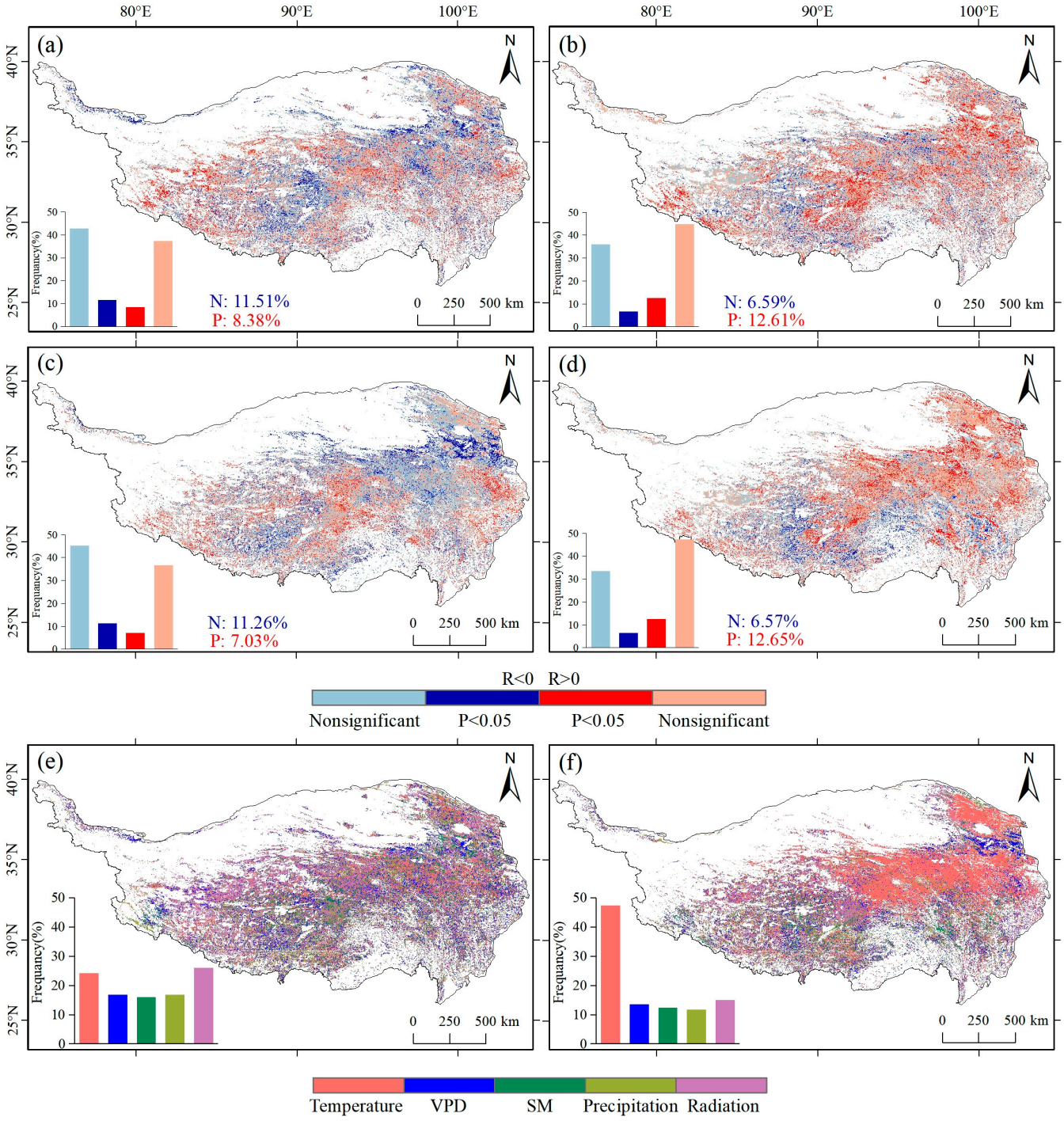

Figure 3. The spatial patterns of the partial correlation coefficients between $NDVI_{max}$ and VPD, and between GPP_{max} and VPD, respectively, after excluding the effects of SM, temperature, precipitation, and radiation (**a**,**c**). The spatial patterns of the partial correlation coefficients between $NDVI_{max}$ and SM, and between GPP_{max} and SM, respectively, after excluding the effects of VPD, temperature, precipitation, and radiation (**b**,**d**). The bar charts represent the respective frequency distributions, and the numbers indicate the proportions of the significant pixels. The spatial patterns of the climate factors correspond to the maximum absolute value of the partial correlation coefficient between $NDVI_{max}$ and GPP_{max} (**e**,**f**), with the bar charts representing the proportion of the pixels for each climate factor.

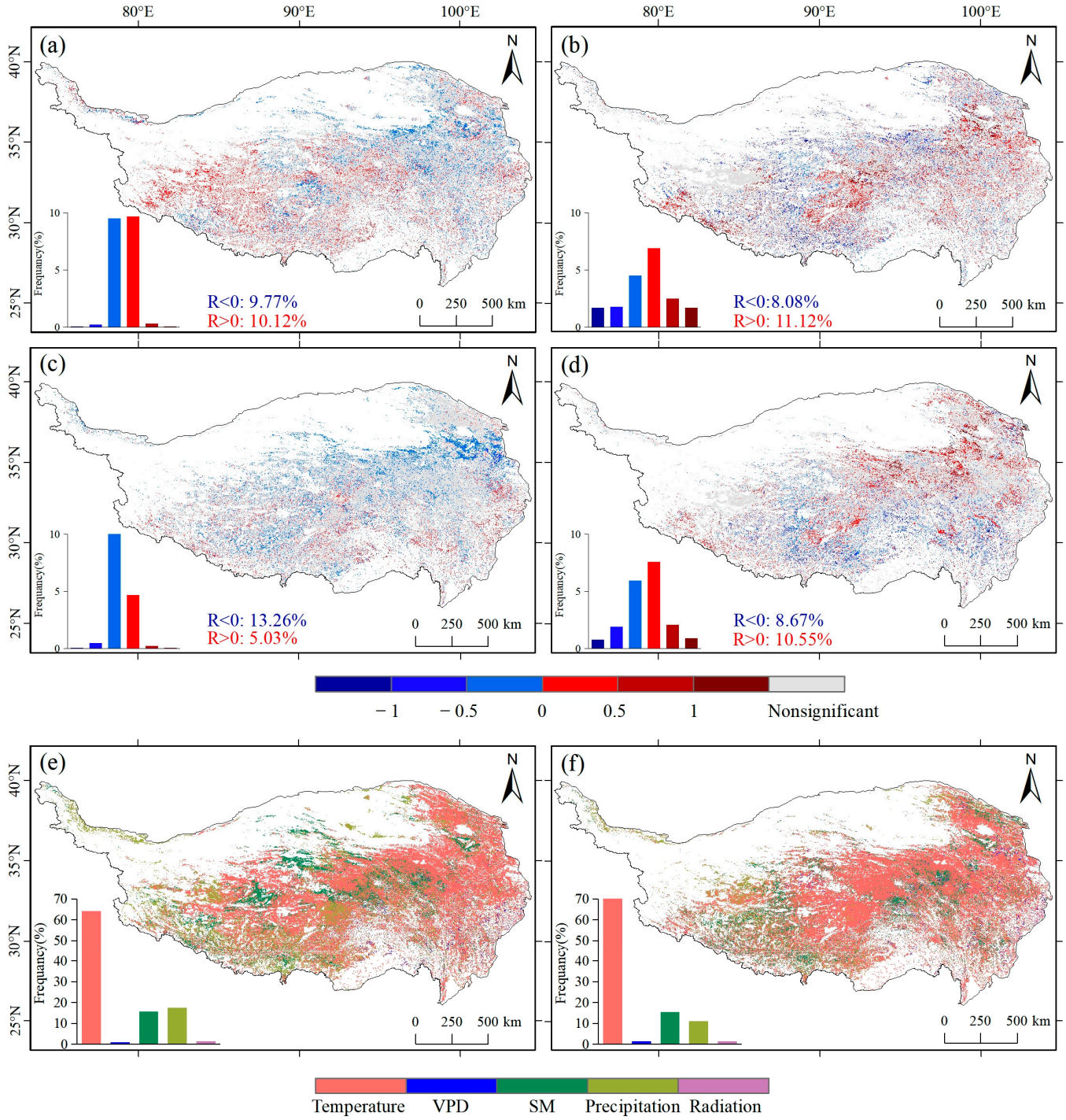

Figure 4. The intensities of the sensitivity of each meteorological factor derived from the ridge regression. The spatial distribution of the sensitivities of $NDVI_{max}$ and GPP_{max} to VPD (**a**,**c**) and the spatial distribution of the sensitivities of $NDVI_{max}$ and GPP_{max} to SM (**b**,**d**). The colored areas in subfigures (**a**–**d**) represent the regions with significant partial correlation coefficients. The spatial patterns of the climate factors correspond to the maximum absolute value of the sensitivity between $NDVI_{max}$ and GPP_{max} (**e**,**f**), with the bar charts representing the proportion of pixels for each climate factor.

In this study, we performed a statistical analysis to examine the correlation between vegetation peak values ($NDVI_{max}$ and GPP_{max}) and climate factors, SM, VPD, temperature, precipitation, and radiation, focusing on four distinct vegetation types: shrub (10.56%),

alpine meadows (25.57%), alpine steppe (27.94%), and alpine sparse vegetation (11.69%). The research findings indicated that among these four vegetation types, more than 57% of the pixels exhibited a positive correlation between $NDVI_{max}$ and SM, with 21% of them showing a noteworthy positive correlation. On the other hand, $NDVI_{max}$ and VPD typically exhibited a negative correlation, accounting for more than 54% of the pixels (see Figure 5a). The patterns of the correlation between GPP_{max} and SM, as well as between GPP_{max} and VPD, closely resembled those observed for $NDVI_{max}$ (Figure 5b). Importantly, there were variations in the correlations between the vegetation peak values and SM and VPD among the vegetation types. In particular, regarding the alpine meadows, close to 60% of the pixels showed a positive correlation between $NDVI_{max}$ and SM, while close to 55% of the pixels exhibited a negative correlation between $NDVI_{max}$ and VPD. This trend held true for GPP_{max}, with slight differences in the pixel distribution, but it was more pronounced in the alpine meadows than in the other vegetation types.

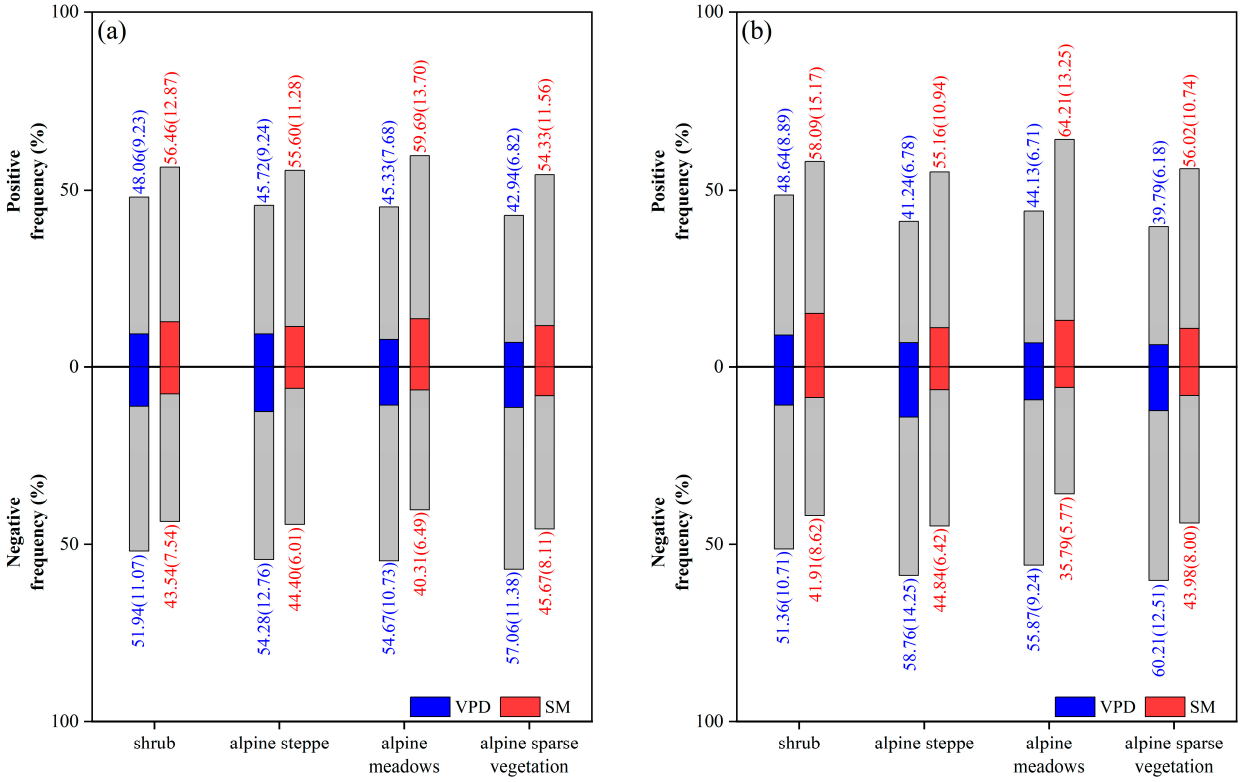

Figure 5. The partial correlation coefficients between the vegetation peak values and the influencing factors at the biome level. (**a**) represents $NDVI_{max}$ and (**b**) represents GPP_{max}. The bar graphs above the zero line show the proportion of positive correlations, whereas those below indicate the proportion of negative correlations. The colored sections indicate the statistically significant correlations ($p < 0.05$), with the numbers in brackets indicating the proportions of these significant correlations.

We observed that $NDVI_{max}$ and GPP_{max} exhibited certain relationships with hydrothermal conditions in terms of their responses to SM and VPD. In areas where the precipitation exceeded 200 mm, $NDVI_{max}$ and VPD exhibited a generally significant negative correlation, particularly in the precipitation ranges of 400–500 mm and 800–900 mm, where the negative correlation coefficients were higher. A positive correlation between $NDVI_{max}$ and VPD was only observed in a small portion of areas where the temperature was below 0 °C and precipitation was less than 200 mm (Figure 6a). Conversely, $NDVI_{max}$ generally showed a positive correlation with SM, with negative correlations appearing only in regions with high temperatures and precipitation (Figure 6b). Additionally, GPP_{max} displayed a pattern similar to $NDVI_{max}$. The evident negative correlation between GPP_{max} and VPD primarily occurred in areas where precipitation ranged from 200 to 600 mm, while a positive partial

correlation was noted when precipitation was between 700 and 800 mm (Figure 6c). Similarly, mirroring the correlation between $NDVI_{max}$ and SM, GPP_{max} showed a significant positive correlation with SM in roughly the same regions, although it demonstrated a negative correlation in areas with higher temperatures and lower precipitation (Figure 6d).

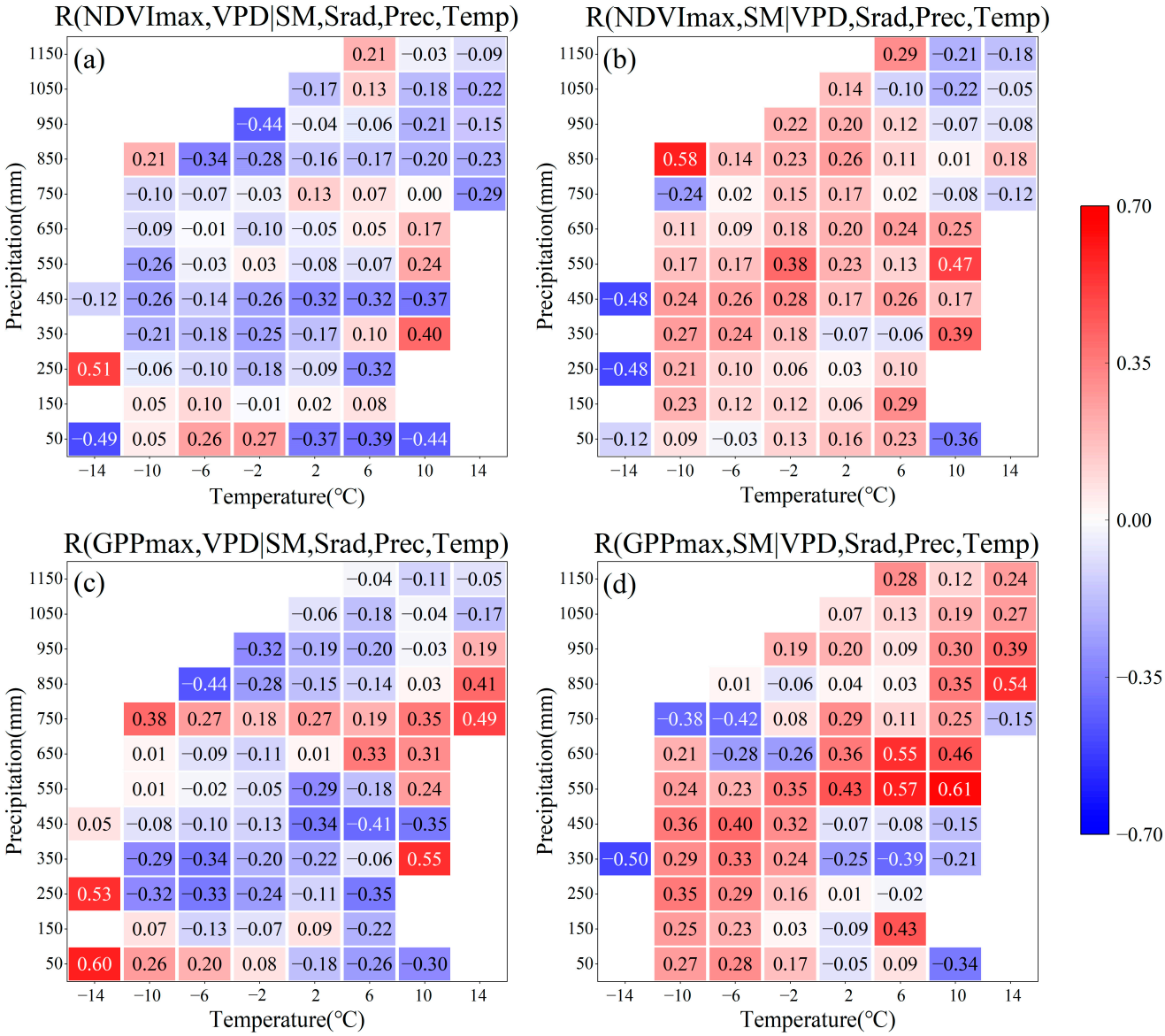

Figure 6. The distribution of mean partial correlation coefficients of $NDVI_{max}$ (**a**) and GPP_{max} (**c**) to VPD along gradients of annual mean temperature and annual total precipitation. The distribution of mean partial correlation coefficients of $NDVI_{max}$ (**b**) and GPP_{max} (**d**) to SM along gradients of annual mean temperature and annual total precipitation.

From Figure 7, it can be observed that the ridge regression coefficients exhibited different results under varying water and heat conditions. In general, the sensitivity of peak vegetation growth to SM was greater than that of VPD. $NDVI_{max}$ showed a significant sensitivity to SM when precipitation was between 400 and 900, while it demonstrated a marked negative sensitivity in areas with precipitation below 400 (Figure 7b). In contrast, $NDVI_{max}$ generally exhibited a negative sensitivity to VPD, but showed a positive sensitivity in areas with precipitation below 200 and above 900 (Figure 7a). GPP_{max} displayed a similar pattern. It showed a positive sensitivity to SM in areas with precipitation below 600, whereas it exhibited a significant negative sensitivity in regions where the temperature was

below −4 °C and precipitation exceeded 600 (Figure 7d). Similarly, GPP_{max} presented a negative sensitivity to VPD in areas with precipitation below 600, while it showed a positive sensitivity in regions where the temperature was above 0° and precipitation exceeded 700 (Figure 7c).

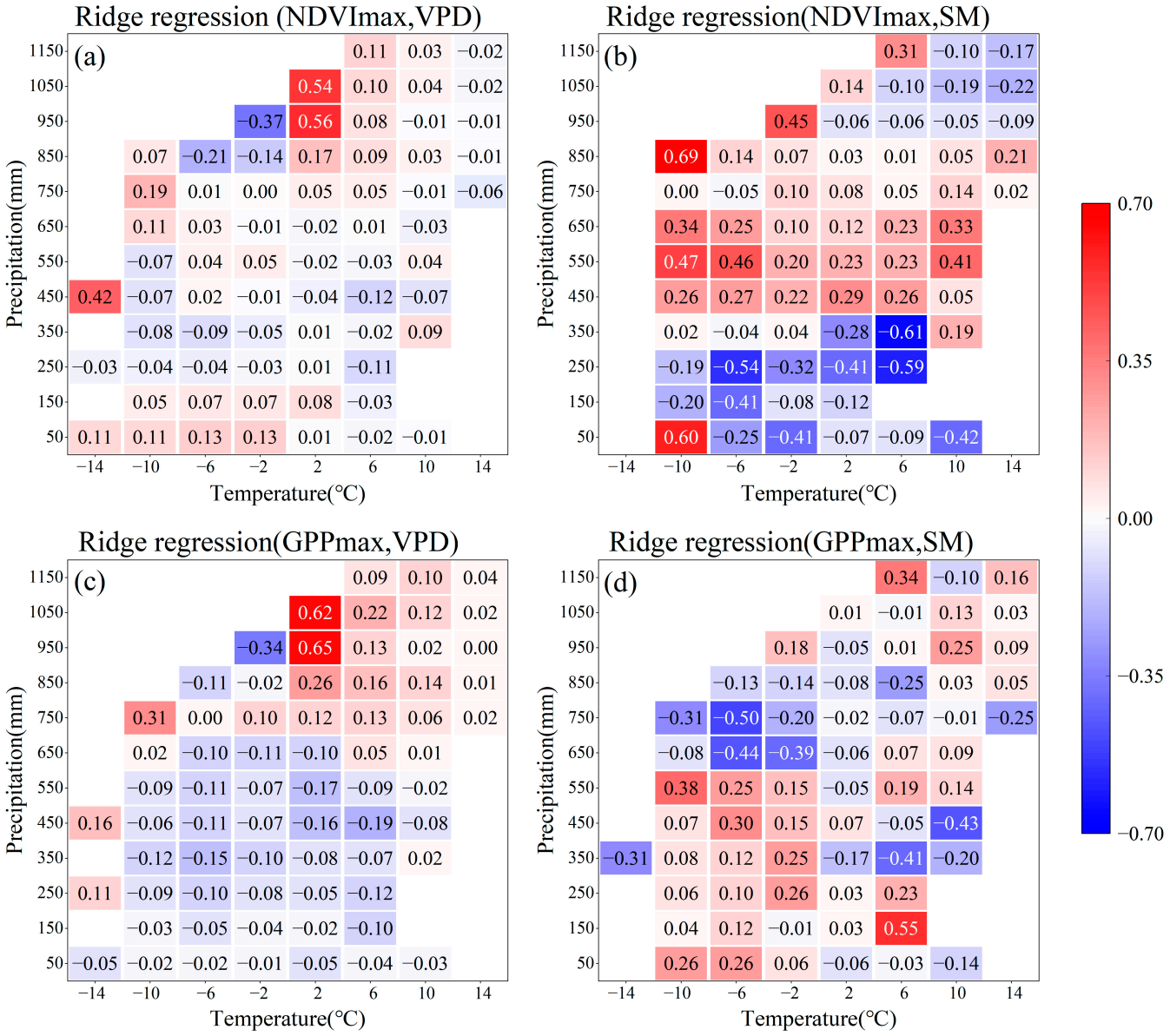

Figure 7. The distribution of mean ridge regression coefficients of $NDVI_{max}$ (**a**) and GPP_{max} (**c**) to VPD along gradients of annual mean temperature and annual total precipitation. The distribution of mean ridge regression coefficients of $NDVI_{max}$ (**b**) and GPP_{max} (**d**) to SM along gradients of annual mean temperature and annual total precipitation.

4. Discussion

4.1. Response of Peak Vegetation Growth to Climate Data

The research findings indicated that there were similar spatial patterns between $NDVI_{max}$ and GPP_{max} on the TP. In most regions, both $NDVI_{max}$ and GPP_{max} showed increasing trends. Approximately 65.28% of the pixels exhibited an increasing tendency for $NDVI_{max}$, with 16.35% showing a significant increase (Figure 2c). Similarly, approximately 72.98% of the pixels showed an increasing tendency for GPP_{max}, with 16.69% displaying a significant increase (Figure 2f). These findings were in line with the one-time observations of widespread and sustained global greening documented in remote sensing studies [14,15,50]. In contrast,

SM and VPD exhibited distinct spatial patterns. From 2000 to 2022, SM decreased in approximately 70.86% of the regions, with approximately 25.82% of the regions displaying a significant decrease (Figure 2i). On the other hand, VPD increased in approximately 74.75% of the regions, with approximately 31.86% of the regions showing a significant increase (Figure 2l). These findings were consistent with previous research indicating that SM and VPD exhibit opposite trends [51].

The evolution of drought involves a complex transition of water resource shortages. It begins with meteorological anomalies such as high atmospheric temperatures, low precipitation, and high evapotranspiration, and continues for a certain period, resulting in abnormal energy transfer within the hydrosphere due to water vapor interactions. Here, it can be seen that the continuous decrease in SM may exacerbate soil drought, and the increase in VPD represents an increase in the atmospheric evaporation demand, which may intensify meteorological drought. However, the formation of drought is influenced by multiple factors and requires more in-depth research.

By studying how SM and VPD affect vegetation peaks, we can observe that $NDVI_{max}$ and GPP_{max} exhibit similar trends. $NDVI_{max}$ is positively correlated with SM and negatively correlated with VPD, and the correlation between them and GPP_{max} is consistent with $NDVI_{max}$. However, overall, the inverse correlation between vegetation peaks and VPD is particularly significant in the northeastern area of the TP. Moreover, the significant positive correlation between vegetation peaks and SM predominates; although the regions vary, they remain largely consistent. This indicates that VPD mainly adversely affects vegetation peaks, while SM helps to promote the growth of vegetation peaks.

On the one hand, SM directly determines the amount of water that plant roots can extract, akin to a reservoir for plants [31]. Thus, SM can directly influence the growth status of the vegetation, subsequently affecting the vegetation peak values. On the other hand, VPD has the potential to prompt plants to close their stomata to decrease water loss [52–55], which could limit the photosynthesis within the ecosystem [31,35]. VPD has a significant impact on the physiological activities of plants. When VPD is high, plants will close the stomata on their leaves to prevent rapid water evaporation. While this behavior helps to reduce water loss, it also hinders the entry of carbon dioxide (CO_2), thereby affecting the efficiency of photosynthesis. Specifically, when VPD exceeds a certain critical value, it will limit the photosynthesis and growth of the plants. In the face of high-VPD conditions, the plants will adjust the opening and closing of stomata to seek a balance between CO_2 absorption and water loss, maintaining a higher photosynthetic rate and thus improving the water use efficiency. In environments with high temperatures and low soil moisture, the constraining effect of VPD on the water and carbon cycles of the ecosystem may be more significant than that of soil moisture [36,37].

Moreover, SM, as a main factor within climate systems, significantly influences biogeochemical cycles, energy, and water [56]. It is also a vital driver of vegetation growth and shows a direct positive correlation with vegetation productivity, which aligns with prior study outcomes [33,57]. Importantly, due to the continuous increase in global temperatures, VPD is also gradually increasing, and it is expected to continue increasing in the future. VPD has become a critical driving factor for plant growth. High-VPD conditions not only suppress the photosynthesis and stomatal conductance in plants, but also increase the water loss through plant transpiration. While the impact of high-VPD conditions may vary among plant species and ecosystems, it may result in reduced primary productivity, exacerbating global drought and leading to plant mortality [58]. This underscores the detrimental influence of VPD on vegetation and explains why vegetation peak values exhibit a negative response to VPD.

4.2. Performance of Partial Correlation Coefficient on Different Vegetation Types

Researchers have shown that the connection between vegetation growth and climate change in the TP region is complex and highly variable. The TP is primarily a high-altitude cold ecosystem where vegetation growth is mostly constrained by the temperature and

precipitation [59–63]. Many scholars have conducted research on the ecosystem of the Tibetan Plateau. Studies have shown that drought has a lagging and cumulative effect on the alpine grasslands of the plateau. Specifically, the response of the alpine meadows to drought is primarily influenced by precipitation, while the response of the alpine grasslands is mainly influenced by the temperature [64]. Additional studies have shown that drought intensity on the Tibetan Plateau impacts the vegetation distribution, with sparse vegetation being the most affected, followed by meadows and grasslands [65]. Other studies have indicated that global warming has intensified the drought risk on the Tibetan Plateau, highlighting that surface temperature is the dominant factor influencing the degree of the vegetation response to drought [28].

With global changes, a good deal of attention has been given to high-altitude meadows and alpine grasslands, while high-altitude sparse vegetation and shrubs have received comparatively less attention. However, it is essential to emphasize that the study of the phenological events in the various vegetation categories on the TP has equal importance [38]. Therefore, we conducted a statistical analysis of these four vegetation types. As depicted in Figure 5, it is evident that the correlation between the vegetation peak values ($NDVI_{max}$, GPP_{max}) and SM and VPD varies among the vegetation types. This illustrates the differences in the ecosystem variations and their responses to driving factors across distinct vegetation categories [38]. The most pronounced response, however, occurs in the alpine meadows, where the vegetation peak values are primarily positively correlated with SM and negatively associated with VPD. This could be a result of the effects of precipitation and temperature on them. The principal grassland variety found on the TP is the alpine meadow [66,67], which has a predominantly cold and humid climate [68]. Many scholars contend that temperature is the influencing factor [66,69–71]. However, some researchers argue that precipitation is its main influencing factor [66,72], and others suggest that it is mostly influenced by spring solar radiation and summer temperatures [66,73]. As shown in Figure 6, the correlations between the vegetation peak values ($NDVI_{max}$ and GPP_{max}) and SM and VPD exhibited more distinct patterns in temperatures ranging from −10 °C to 10 °C and precipitation levels between 200 and 800 mm. This further underscores the critical importance of precipitation and temperature influences.

4.3. Response of SM and VPD to Vegetation Growth Peak Under Different Hydrothermal Conditions

Broadly speaking, elevated VPD and reduced SM typically hinder vegetation growth. However, an opposite trend is shown in some regions in Figure 6, where VPD is positively correlated and SM is negatively correlated. First, SM exhibited a negative correlation in areas with higher precipitation levels. This can be explained from two major perspectives. Firstly, a moderate increase in precipitation can directly enhance soil moisture, making it more favorable for plant growth and resulting in a positive correlation between the vegetation peak values and SM. In addition, excessive rainfall may lead to a reduction in solar radiation, thus impacting the photosynthesis in plants and consequently decreasing the vegetation peak values [74–77]. Secondly, with the gradual warming of the global climate, the corresponding increase in VPD is notable. VPD not only hinders plant photosynthesis and stomatal conductance, but also elevates plant transpirational water loss, thereby negatively impacting the vegetation peak values [58]. However, Figure 6 shows that some regions exhibit opposite trends in VPD, while the regions with positive correlations in VPD are mostly concentrated in areas with higher temperatures and precipitation. The main reason may be that the increase in VPD promotes photosynthesis when the temperature is suitable and the water availability is sufficient.

Due to VPD's regulation of plant stomata, plants will close their stomata to reduce water loss when VPD is high. However, this closure also limits the absorption of CO_2 by the plants, leading to a decrease in photosynthesis and affecting the peak growth of the vegetation [31]. On the one hand, when the temperature rises, it leads to an increase in VPD, which in turn reduces the photosynthesis of the vegetation [58]. Higher temperatures

also accelerate water evaporation, thereby reducing SM. Additionally, low soil moisture and high VPD both limit the photosynthesis of the vegetation [36]. On the other hand, increased precipitation enhances SM, and the subsequent rise in evapotranspiration reduces VPD, thereby promoting the photosynthesis of the vegetation [78]. However, even with sufficient precipitation, rising temperatures can lead to increased evapotranspiration, thereby inhibiting plant growth. Conversely, plants will not experience water stress when the precipitation is insufficient as long as the temperature is suitable [79]. Therefore, the multifaceted impacts of SM and VPD on vegetation under varying temperature and precipitation conditions warrant further exploration. From the results of this study, it is found that SM and VPD follow established patterns in their effects on vegetation when temperature and precipitation are within normal ranges; however, they exhibit completely opposite effects under certain extreme conditions.

4.4. Limitations of the Research

Of course, since we only selected SM, VPD, temperature, precipitation, and radiation as influencing factors to study the trends of vegetation peak changes, we may lack a complete explanation of the reasons behind these changes. Moreover, precipitation is the main source of SM and plays a crucial role in SM. At the same time, it can also cause changes in air humidity, thereby affecting VPD. However, different precipitation patterns often have different effects, which were not considered in this article. In future research endeavors, it would be beneficial to investigate a wider range of influencing factors to arrive at a more precise understanding of the causes of vegetation peak value changes. This would enable a more comprehensive description of the major factors affecting vegetation growth, providing valuable guidance for the ecological management of the TP. Furthermore, the data used in this research may have limitations, and it is preferable to draw conclusions based on long-term research. The reliability of the final conclusions can be ensured through further in-depth analysis of the influencing mechanisms via detailed ground experiments.

5. Conclusions

We based this article on satellite greening data and meteorological datasets from 2001 to 2022 and used Theil–Sen media trend analysis and partial correlation analysis to study the spatiotemporal changes in $NDVI_{max}$, GPP_{max}, SM, and saturated VPD in the TP, as well as the response of the first two to the latter two. The results indicate that $NDVI_{max}$ and GPP_{max} have similar spatial patterns, with $NDVI_{max}$ and GPP_{max} showing an upward trend in most regions, accounting for approximately 65% of the area; SM and VPD exhibit different multiyear average spatial patterns, with SM showing a downward trend in 70% of the region, while VPD shows the opposite trend, with approximately 70% of the region showing an upward trend. Our findings indicate that both $NDVI_{max}$ and GPP_{max} exhibit positive correlations with SM and negative correlations with VPD, attributable to the influence of driving factors. From the results of the partial correlation coefficient, it can be seen that the correlation between SM and VPD on peak vegetation growth is as important as precipitation and radiation. Furthermore, the results of the analysis of sensitivity intensity further support the importance of SM to the peak of vegetation growth.

From the perspective of statistical vegetation types, the above correlation patterns were also observed in the four vegetation types of shrubs, alpine grasslands, alpine meadows, and sparse alpine vegetation. The most obvious manifestation was in the alpine meadows, which showed a dominant advantage over vegetation growth peaks in 60% of the areas. From the perspective of hydrothermal conditions, the above correlation pattern was only observed in areas with precipitation ranging from 200 to 800 mm and temperatures ranging from −10 °C to 10 °C. When precipitation is too high, the peak vegetation values will be positively correlated with VPD, and conversely, they will be negatively correlated with SM. Overall, SM helps to promote the growth of vegetation peaks, while VPD mainly adversely affects vegetation peaks. Against the backdrop of global climate change, frequent drought events mean that the vegetation of the TP is facing a gradually worsening environment. This

study contributes to a more comprehensive understanding of how vegetation phenology responds to future climate change.

Author Contributions: Conceptualization, X.W.; data curation, Z.Q.; methodology, Z.Q. and X.W.; writing—original draft, Z.Q. and L.T.; writing—review and editing, X.W., Y.Z., J.T., J.Y. and S.X. All authors have read and agreed to the published version of the manuscript.

Funding: This research was funded by the National Key R&D program of China (Grant No. 2023YFF1303804), the National Natural Science Foundation of China (Grant No. 42271034), and the Youth Innovation Promotion Association of Chinese Academy of Sciences (Grant No. 2022051).

Data Availability Statement: The NDVI and GPP data were obtained from the NASA Earthdata Cloud website (https://appeears.earthdatacloud.nasa.gov/, accessed on 12 December 2023). The climate data were obtained from the TerraClimate dataset (https://www.climatologylab.org/terraclimate.html, accessed on 12 December 2023).

Conflicts of Interest: The authors declare no conflicts of interest.

References

1. Gao, Q.; Guo, Y.; Xu, H.; Ganjurjav, H.; Li, Y.; Wan, Y.; Qin, X.; Ma, X.; Liu, S. Climate change and its impacts on vegetation distribution and net primary productivity of the alpine ecosystem in the Qinghai-Tibetan Plateau. *Sci. Total Environ.* **2016**, *554*, 34–41. [CrossRef] [PubMed]
2. Yao, T.; Bolch, T.; Chen, D.; Gao, J.; Immerzeel, W.; Piao, S.; Su, F.; Thompson, L.; Wada, Y.; Wang, L. The imbalance of the Asian water tower. *Nat. Rev. Earth Environ.* **2022**, *3*, 618–632. [CrossRef]
3. Zhao, D.; Zhu, Y.; Wu, S.; Zheng, D. Projection of vegetation distribution to 1.5 C and 2 C of global warming on the Tibetan Plateau. *Glob. Planet. Chang.* **2021**, *202*, 103525. [CrossRef]
4. Bai, Y.; Guo, C.; Degen, A.A.; Ahmad, A.A.; Wang, W.; Zhang, T.; Li, W.; Ma, L.; Huang, M.; Zeng, H. Climate warming benefits alpine vegetation growth in Three-River Headwater Region, China. *Sci. Total Environ.* **2020**, *742*, 140574. [CrossRef]
5. Wang, Y.; Ma, Y.; Li, H.; Yuan, L. Carbon and water fluxes and their coupling in an alpine meadow ecosystem on the northeastern Tibetan Plateau. *Theor. Appl. Climatol.* **2020**, *142*, 1–18. [CrossRef]
6. Li, H.; Zhu, J.; Zhang, F.; He, H.; Yang, Y.; Li, Y.; Cao, G.; Zhou, H. Growth stage-dependant variability in water vapor and CO_2 exchanges over a humid alpine shrubland on the northeastern Qinghai-Tibetan Plateau. *Agric. For. Meteorol.* **2019**, *268*, 55–62. [CrossRef]
7. Saito, M.; Kato, T.; Tang, Y. Temperature controls ecosystem CO_2 exchange of an alpine meadow on the northeastern Tibetan Plateau. *Glob. Chang. Biol.* **2009**, *15*, 221–228. [CrossRef]
8. Vanneste, T.; Michelsen, O.; Graae, B.J.; Kyrkjeeide, M.O.; Holien, H.; Hassel, K.; Lindmo, S.; Kapás, R.E.; De Frenne, P. Impact of climate change on alpine vegetation of mountain summits in Norway. *Ecol. Res.* **2017**, *32*, 579–593. [CrossRef]
9. Ahlström, A.; Raupach, M.R.; Schurgers, G.; Smith, B.; Arneth, A.; Jung, M.; Reichstein, M.; Canadell, J.G.; Friedlingstein, P.; Jain, A.K. The dominant role of semi-arid ecosystems in the trend and variability of the land CO_2 sink. *Science* **2015**, *348*, 895–899. [CrossRef]
10. Forkel, M.; Carvalhais, N.; Rödenbeck, C.; Keeling, R.; Heimann, M.; Thonicke, K.; Zaehle, S.; Reichstein, M. Enhanced seasonal CO_2 exchange caused by amplified plant productivity in northern ecosystems. *Science* **2016**, *351*, 696–699. [CrossRef]
11. Graven, H.; Keeling, R.; Piper, S.; Patra, P.; Stephens, B.; Wofsy, S.; Welp, L.; Sweeney, C.; Tans, P.; Kelley, J. Enhanced seasonal exchange of CO_2 by northern ecosystems since 1960. *Science* **2013**, *341*, 1085–1089. [CrossRef] [PubMed]
12. Huang, K.; Xia, J.; Wang, Y.; Ahlström, A.; Chen, J.; Cook, R.B.; Cui, E.; Fang, Y.; Fisher, J.B.; Huntzinger, D.N. Enhanced peak growth of global vegetation and its key mechanisms. *Nat. Ecol. Evol.* **2018**, *2*, 1897–1905. [CrossRef] [PubMed]
13. Xia, J.; Niu, S.; Ciais, P.; Janssens, I.A.; Chen, J.; Ammann, C.; Arain, A.; Blanken, P.D.; Cescatti, A.; Bonal, D. Joint control of terrestrial gross primary productivity by plant phenology and physiology. *Proc. Natl. Acad. Sci. USA* **2015**, *112*, 2788–2793. [CrossRef] [PubMed]
14. Zhu, Z.; Piao, S.; Myneni, R.B.; Huang, M.; Zeng, Z.; Canadell, J.G.; Ciais, P.; Sitch, S.; Friedlingstein, P.; Arneth, A. Greening of the Earth and its drivers. *Nat. Clim. Chang.* **2016**, *6*, 791–795. [CrossRef]
15. Chen, C.; Park, T.; Wang, X.; Piao, S.; Xu, B.; Chaturvedi, R.K.; Fuchs, R.; Brovkin, V.; Ciais, P.; Fensholt, R. China and India lead in greening of the world through land-use management. *Nat. Sustain.* **2019**, *2*, 122–129. [CrossRef]
16. Xu, C.; Liu, H.; Williams, A.P.; Yin, Y.; Wu, X. Trends toward an earlier peak of the growing season in Northern Hemisphere mid-latitudes. *Glob. Chang. Biol.* **2016**, *22*, 2852–2860. [CrossRef]
17. Yang, J.; Dong, J.; Xiao, X.; Dai, J.; Wu, C.; Xia, J.; Zhao, G.; Zhao, M.; Li, Z.; Zhang, Y. Divergent shifts in peak photosynthesis timing of temperate and alpine grasslands in China. *Remote Sens. Environ.* **2019**, *233*, 111395. [CrossRef]
18. Liu, Y.; Wu, C.; Wang, X.; Jassal, R.S.; Gonsamo, A. Impacts of global change on peak vegetation growth and its timing in terrestrial ecosystems of the continental US. *Glob. Planet. Chang.* **2021**, *207*, 103657. [CrossRef]

19. Buermann, W.; Bikash, P.R.; Jung, M.; Burn, D.H.; Reichstein, M. Earlier springs decrease peak summer productivity in North American boreal forests. *Environ. Res. Lett.* **2013**, *8*, 024027. [CrossRef]
20. Gonsamo, A.; Chen, J.M.; Ooi, Y.W. Peak season plant activity shift towards spring is reflected by increasing carbon uptake by extratropical ecosystems. *Glob. Chang. Biol.* **2018**, *24*, 2117–2128. [CrossRef]
21. He, P.; Sun, Z.; Xu, D.; Liu, H.; Yao, R.; Ma, J. Combining gradual and abrupt analysis to detect variation of vegetation greenness on the loess areas of China. *Front. Earth Sci.* **2021**, *16*, 368–380. [CrossRef]
22. Liu, Y.; Wu, C.; Wang, X.; Zhang, Y. Contrasting responses of peak vegetation growth to asymmetric warming: Evidences from FLUXNET and satellite observations. *Glob. Chang. Biol.* **2023**, *29*, 2363–2379. [CrossRef]
23. Du, C.; Chen, J.; Nie, T.; Dai, C. Spatial–temporal changes in meteorological and agricultural droughts in Northeast China: Change patterns, response relationships and causes. *Nat. Hazards* **2022**, *110*, 155–173. [CrossRef]
24. Feng, W.; Lu, H.; Yao, T.; Yu, Q. Drought characteristics and its elevation dependence in the Qinghai–Tibet plateau during the last half-century. *Sci. Rep.* **2020**, *10*, 14323. [CrossRef] [PubMed]
25. Fang, W.; Huang, S.; Huang, Q.; Huang, G.; Wang, H.; Leng, G.; Wang, L.; Guo, Y. Probabilistic assessment of remote sensing-based terrestrial vegetation vulnerability to drought stress of the Loess Plateau in China. *Remote Sens. Environ.* **2019**, *232*, 111290. [CrossRef]
26. Jinsong, W.; Yubi, Y.; Ying, W.; Suping, W.; Xiaoyun, L.; Yue, Z.; Haolin, D.; Yu, Z.; Yulong, R. Meteorological droughts in the Qinghai-Tibet Plateau: Research progress and prospects. *Adv. Earth Sci.* **2022**, *37*, 441.
27. Wu, D.; Hu, Z. Increasing compound drought and hot event over the Tibetan Plateau and its effects on soil water. *Ecol. Indic.* **2023**, *153*, 110413. [CrossRef]
28. Wang, Y.; Fu, B.; Liu, Y.; Li, Y.; Feng, X.; Wang, S. Response of vegetation to drought in the Tibetan Plateau: Elevation differentiation and the dominant factors. *Agric. For. Meteorol.* **2021**, *306*, 108468. [CrossRef]
29. Wu, C.; Peng, J.; Ciais, P.; Peñuelas, J.; Wang, H.; Beguería, S.; Andrew Black, T.; Jassal, R.S.; Zhang, X.; Yuan, W. Increased drought effects on the phenology of autumn leaf senescence. *Nat. Clim. Chang.* **2022**, *12*, 943–949. [CrossRef]
30. Zhao, C.; Brissette, F.; Chen, J. Projection of future extreme meteorological droughts using two large multi-member climate model ensembles. *J. Hydrol.* **2023**, *618*, 129155. [CrossRef]
31. Liu, L.; Gudmundsson, L.; Hauser, M.; Qin, D.; Li, S.; Seneviratne, S.I. Soil moisture dominates dryness stress on ecosystem production globally. *Nat. Commun.* **2020**, *11*, 4892. [CrossRef] [PubMed]
32. Zhou, S.; Williams, A.P.; Berg, A.M.; Cook, B.I.; Zhang, Y.; Hagemann, S.; Lorenz, R.; Seneviratne, S.I.; Gentine, P. Land–atmosphere feedbacks exacerbate concurrent soil drought and atmospheric aridity. *Proc. Natl. Acad. Sci. USA* **2019**, *116*, 18848–18853. [CrossRef] [PubMed]
33. Zhang, W.; Wei, F.; Horion, S.; Fensholt, R.; Forkel, M.; Brandt, M. Global quantification of the bidirectional dependency between soil moisture and vegetation productivity. *Agric. For. Meteorol.* **2022**, *313*, 108735. [CrossRef]
34. Lu, H.; Qin, Z.; Lin, S.; Chen, X.; Chen, B.; He, B.; Wei, J.; Yuan, W. Large influence of atmospheric vapor pressure deficit on ecosystem production efficiency. *Nat. Commun.* **2022**, *13*, 1653. [CrossRef]
35. Zhong, Z.; He, B.; Wang, Y.-P.; Chen, H.W.; Chen, D.; Fu, Y.H.; Chen, Y.; Guo, L.; Deng, Y.; Huang, L. Disentangling the effects of vapor pressure deficit on northern terrestrial vegetation productivity. *Sci. Adv.* **2023**, *9*, eadf3166. [CrossRef]
36. Qi, G.; She, D.; Xia, J.; Song, J.; Jiao, W.; Li, J.; Liu, Z. Soil moisture plays an increasingly important role role in constraining vegetation productivity in China over the past two decades. *Agric. For. Meteorol.* **2024**, *356*, 110193. [CrossRef]
37. Tu, Y.; Wang, X.; Zhou, J.; Wang, X.; Jia, Z.; Ma, J.; Yao, W.; Zhang, X.; Sun, Z.; Luo, P. Atmospheric water demand dominates terrestrial ecosystem productivity in China. *Agric. For. Meteorol.* **2024**, *355*, 110151. [CrossRef]
38. Peng, J.; Wu, C.; Wang, X.; Lu, L. Spring phenology outweighed climate change in determining autumn phenology on the Tibetan Plateau. *Int. J. Climatol.* **2021**, *41*, 3725–3742. [CrossRef]
39. Shen, M.; Zhang, G.; Cong, N.; Wang, S.; Kong, W.; Piao, S. Increasing altitudinal gradient of spring vegetation phenology during the last decade on the Qinghai–Tibetan Plateau. *Agric. For. Meteorol.* **2014**, *189*, 71–80. [CrossRef]
40. Wang, X.; Wu, C.; Liu, Y.; Peñuelas, J.; Peng, J. Earlier leaf senescence dates are constrained by soil moisture. *Glob. Chang. Biol.* **2023**, *29*, 1557–1573. [CrossRef]
41. Abatzoglou, J.T.; Dobrowski, S.Z.; Parks, S.A.; Hegewisch, K.C. TerraClimate, a high-resolution global dataset of monthly climate and climatic water balance from 1958–2015. *Sci. Data* **2018**, *5*, 170191. [CrossRef] [PubMed]
42. Liu, Y.; Wu, C.; Jassal, R.S.; Wang, X.; Shang, R. Satellite observed land surface greening in summer controlled by the precipitation frequency rather than its total over Tibetan Plateau. *Earth's Future* **2022**, *10*, e2022EF002760. [CrossRef]
43. Shen, M.; Tang, Y.; Chen, J.; Zhu, X.; Zheng, Y. Influences of temperature and precipitation before the growing season on spring phenology in grasslands of the central and eastern Qinghai-Tibetan Plateau. *Agric. For. Meteorol.* **2011**, *151*, 1711–1722. [CrossRef]
44. Yu, F.; Price, K.P.; Ellis, J.; Shi, P. Response of seasonal vegetation development to climatic variations in eastern central Asia. *Remote Sens. Environ.* **2003**, *87*, 42–54. [CrossRef]
45. Liu, W.; Mo, X.; Liu, S.; Lin, Z.; Lv, C. Attributing the changes of grass growth, water consumed and water use efficiency over the Tibetan Plateau. *J. Hydrol.* **2021**, *598*, 126464. [CrossRef]
46. Hoerl, A.E.; Kennard, R.W. Ridge regression: Biased estimation for nonorthogonal problems. *Technometrics* **1970**, *12*, 55–67. [CrossRef]

47. Zhao, Y.; Chen, Y.; Wu, C.; Li, G.; Ma, M.; Fan, L.; Zheng, H.; Song, L.; Tang, X. Exploring the contribution of environmental factors to evapotranspiration dynamics in the Three-River-Source region, China. *J. Hydrol.* **2023**, *626*, 130222. [CrossRef]
48. Golub, G.H.; Heath, M.; Wahba, G. Generalized cross-validation as a method for choosing a good ridge parameter. *Technometrics* **1979**, *21*, 215–223. [CrossRef]
49. Lu, J.; Wang, G.; Li, S.; Feng, A.; Zhan, M.; Jiang, T.; Su, B.; Wang, Y. Projected land evaporation and its response to vegetation greening over China under multiple scenarios in the CMIP6 models. *J. Geophys. Res. Biogeosci.* **2021**, *126*, e2021JG006327. [CrossRef]
50. Piao, S.; Friedlingstein, P.; Ciais, P.; Zhou, L.; Chen, A. Effect of climate and CO_2 changes on the greening of the Northern Hemisphere over the past two decades. *Geophys. Res. Lett.* **2006**, *33*, L23402. [CrossRef]
51. Zhao, D.; Zhang, Z.; Zhang, Y. Soil Moisture Dominates the Forest Productivity Decline During the 2022 China Compound Drought-Heatwave Event. *Geophys. Res. Lett.* **2023**, *50*, e2023GL104539. [CrossRef]
52. Liu, L.; Peng, S.; AghaKouchak, A.; Huang, Y.; Li, Y.; Qin, D.; Xie, A.; Li, S. Broad consistency between satellite and vegetation model estimates of net primary productivity across global and regional scales. *J. Geophys. Res. Biogeosci.* **2018**, *123*, 3603–3616. [CrossRef]
53. Oren, R.; Sperry, J.; Katul, G.; Pataki, D.; Ewers, B.; Phillips, N.; Schäfer, K. Survey and synthesis of intra- and interspecific variation in stomatal sensitivity to vapour pressure deficit. *Plant Cell Environ.* **1999**, *22*, 1515–1526. [CrossRef]
54. Stocker, B.D.; Zscheischler, J.; Keenan, T.F.; Prentice, I.C.; Peñuelas, J.; Seneviratne, S.I. Quantifying soil moisture impacts on light use efficiency across biomes. *New Phytol.* **2018**, *218*, 1430–1449. [CrossRef]
55. Williams, A.P.; Allen, C.D.; Millar, C.I.; Swetnam, T.W.; Michaelsen, J.; Still, C.J.; Leavitt, S.W. Forest responses to increasing aridity and warmth in the southwestern United States. *Proc. Natl. Acad. Sci. USA* **2010**, *107*, 21289–21294. [CrossRef]
56. Seneviratne, S.I.; Corti, T.; Davin, E.L.; Hirschi, M.; Jaeger, E.B.; Lehner, I.; Orlowsky, B.; Teuling, A.J. Investigating soil moisture–climate interactions in a changing climate: A review. *Earth-Sci. Rev.* **2010**, *99*, 125–161. [CrossRef]
57. Huber, S.; Fensholt, R.; Rasmussen, K. Water availability as the driver of vegetation dynamics in the African Sahel from 1982 to 2007. *Glob. Planet. Chang.* **2011**, *76*, 186–195. [CrossRef]
58. Grossiord, C.; Buckley, T.N.; Cernusak, L.A.; Novick, K.A.; Poulter, B.; Siegwolf, R.T.; Sperry, J.S.; McDowell, N.G. Plant responses to rising vapor pressure deficit. *New Phytol.* **2020**, *226*, 1550–1566. [CrossRef]
59. Shen, M.; Piao, S.; Dorji, T.; Liu, Q.; Cong, N.; Chen, X.; An, S.; Wang, S.; Wang, T.; Zhang, G. Plant phenological responses to climate change on the Tibetan Plateau: Research status and challenges. *Natl. Sci. Rev.* **2015**, *2*, 454–467. [CrossRef]
60. Li, J.; Wu, C.; Wang, X.; Peng, J.; Dong, D.; Lin, G.; Gonsamo, A. Satellite observed indicators of the maximum plant growth potential and their responses to drought over Tibetan Plateau (1982–2015). *Ecol. Indic.* **2020**, *108*, 105732. [CrossRef]
61. Shen, M.; Piao, S.; Jeong, S.-J.; Zhou, L.; Zeng, Z.; Ciais, P.; Chen, D.; Huang, M.; Jin, C.-S.; Li, L.Z. Evaporative cooling over the Tibetan Plateau induced by vegetation growth. *Proc. Natl. Acad. Sci. USA* **2015**, *112*, 9299–9304. [CrossRef] [PubMed]
62. Yu, H.; Luedeling, E.; Xu, J. Winter and spring warming result in delayed spring phenology on the Tibetan Plateau. *Proc. Natl. Acad. Sci. USA* **2010**, *107*, 22151–22156. [CrossRef] [PubMed]
63. Cong, N.; Shen, M.; Yang, W.; Yang, Z.; Zhang, G.; Piao, S. Varying responses of vegetation activity to climate changes on the Tibetan Plateau grassland. *Int. J. Biometeorol.* **2017**, *61*, 1433–1444. [CrossRef] [PubMed]
64. Wang, X.; Hu, Z.; Zhang, Z.; Tang, J.; Niu, B. Altitude-Shifted Climate Variables Dominate the Drought Effects on Alpine Grasslands over the Qinghai–Tibetan Plateau. *Sustainability* **2024**, *16*, 6697. [CrossRef]
65. Li, X.; Pan, Y. The Impacts of Drought Changes on Alpine Vegetation during the Growing Season over the Tibetan Plateau in 1982–2018. *Remote Sens.* **2024**, *16*, 1909. [CrossRef]
66. Hao, A.; Duan, H.; Wang, X.; Zhao, G.; You, Q.; Peng, F.; Du, H.; Liu, F.; Li, C.; Lai, C. Different response of alpine meadow and alpine steppe to climatic and anthropogenic disturbance on the Qinghai-Tibetan Plateau. *Glob. Ecol. Conserv.* **2021**, *27*, e01512. [CrossRef]
67. Zhang, G.; Zhang, Y.; Dong, J.; Xiao, X. Green-up dates in the Tibetan Plateau have continuously advanced from 1982 to 2011. *Proc. Natl. Acad. Sci. USA* **2013**, *110*, 4309–4314. [CrossRef]
68. Wang, X.; Yi, S.; Wu, Q.; Yang, K.; Ding, Y. The role of permafrost and soil water in distribution of alpine grassland and its NDVI dynamics on the Qinghai-Tibetan Plateau. *Glob. Planet. Chang.* **2016**, *147*, 40–53. [CrossRef]
69. Ganjurjav, H.; Gao, Q.; Gornish, E.S.; Schwartz, M.W.; Liang, Y.; Cao, X.; Zhang, W.; Zhang, Y.; Li, W.; Wan, Y. Differential response of alpine steppe and alpine meadow to climate warming in the central Qinghai–Tibetan Plateau. *Agric. For. Meteorol.* **2016**, *223*, 233–240. [CrossRef]
70. Wang, Y.; Wesche, K. Vegetation and soil responses to livestock grazing in Central Asian grasslands: A review of Chinese literature. *Biodivers. Conserv.* **2016**, *25*, 2401–2420. [CrossRef]
71. Zhang, L.; Guo, H.; Wang, C.; Ji, L.; Li, J.; Wang, K.; Dai, L. The long-term trends (1982–2006) in vegetation greenness of the alpine ecosystem in the Qinghai-Tibetan Plateau. *Environ. Earth Sci.* **2014**, *72*, 1827–1841. [CrossRef]
72. Sun, J.; Qin, X.; Yang, J. The response of vegetation dynamics of the different alpine grassland types to temperature and precipitation on the Tibetan Plateau. *Environ. Monit. Assess.* **2016**, *188*, 20. [CrossRef] [PubMed]
73. Zheng, Z.; Zhu, W.; Zhang, Y. Seasonally and spatially varied controls of climatic factors on net primary productivity in alpine grasslands on the Tibetan Plateau. *Glob. Ecol. Conserv.* **2020**, *21*, e00814. [CrossRef]

74. Liu, Q.; Fu, Y.H.; Zeng, Z.; Huang, M.; Li, X.; Piao, S. Temperature, precipitation, and insolation effects on autumn vegetation phenology in temperate China. *Glob. Chang. Biol.* **2016**, *22*, 644–655. [CrossRef]
75. Shen, M.; Piao, S.; Cong, N.; Zhang, G.; Jassens, I.A. Precipitation impacts on vegetation spring phenology on the Tibetan Plateau. *Glob. Chang. Biol.* **2015**, *21*, 3647–3656. [CrossRef]
76. Wang, X.; Wu, C. Estimating the peak of growing season (POS) of China's terrestrial ecosystems. *Agric. For. Meteorol.* **2019**, *278*, 107639. [CrossRef]
77. Wu, C.; Chen, J.M.; Desai, A.R.; Lafleur, P.M.; Verma, S.B. Positive impacts of precipitation intensity on monthly CO_2 fluxes in North America. *Glob. Planet. Chang.* **2013**, *100*, 204–214. [CrossRef]
78. Fu, Z.; Ciais, P.; Prentice, I.C.; Gentine, P.; Makowski, D.; Bastos, A.; Luo, X.; Green, J.K.; Stoy, P.C.; Yang, H. Atmospheric dryness reduces photosynthesis along a large range of soil water deficits. *Nat. Commun.* **2022**, *13*, 989. [CrossRef]
79. Ma, C.; Wang, X.; Wu, C. Early leaf senescence under drought conditions in the Northern hemisphere. *Agric. For. Meteorol.* **2024**, *358*, 110231. [CrossRef]